THE JOURNAL OF PHYSICAL CHEMISTRY C

Article

pubs.acs.org/JPCC

New Mechanism for Oxidation of Native Silicon Oxide

U. Khalilov,*[,†] G. Pourtois,[†,‡] S. Huygh,[†] A. C. T. van Duin,[§] E. C. Neyts,[†] and A. Bogaerts[†]

[†]PLASMANT Research Group, Department of Chemistry, University of Antwerp, Universiteitsplein 1, 2610 Antwerp, Belgium

[‡]IMEC, Kapeldreef 75, 3001 Leuven, Belgium

[§]Department of Mechanical and Nuclear Engineering, Pennsylvania State University, University Park, Pennsylvania 16801, United States

ABSTRACT: Continued miniaturization of metal-oxide-semiconductor field-effect transistors (MOSFETs) requires an ever-decreasing thickness of the gate oxide. The structure of ultrathin silicon oxide films, however, critically depends on the oxidation mechanism. Using reactive atomistic simulations, we here demonstrate how the oxidation mechanism in hyperthermal oxidation of such structures may be controlled by the oxidation temperature and the oxidant energy. Specifically, we study the interaction of hyperthermal oxygen with energies of 1−5 eV with thin SiO_x ($x \leq 2$) films with a native oxide thickness of about 10 Å. We analyze the oxygen penetration depth probability and compare with results of the hyperthermal oxidation of a bare Si(100){2 × 1} (*c*-Si) surface. The temperature-dependent oxidation mechanisms are discussed in detail. Our results demonstrate that, at low (i.e., room) temperature, the penetrated oxygen mostly resides in the oxide region rather than at the SiO_x|*c*-Si interface. However, at higher temperatures, starting at around 700 K, oxygen atoms are found to penetrate and to diffuse through the oxide layer followed by reaction at the *c*-Si boundary. We demonstrate that hyperthermal oxidation resembles thermal oxidation, which can be described by the Deal−Grove model at high temperatures. Furthermore, defect creation mechanisms that occur during the oxidation process are also analyzed. This study is useful for the fabrication of ultrathin silicon oxide gate oxides for metal-oxide-semiconductor devices as it links parameters that can be straightforwardly controlled in experiment (oxygen temperature, velocity) with the silicon oxide structure.

■ INTRODUCTION

The current gate thickness is close to the fundamental limit,[1] and thus, understanding at the atomic scale and controlling the thickness as well as the quality of such ultrathin oxide films becomes even more crucial.[2,3] Hyperthermal oxidation of silicon as an alternative to thermal oxidation is envisaged for semiconductor applications because of its ability to control such oxide thickness.[4] Although numerous studies have elucidated the overall hyperthermal oxidation behavior, most investigations have been carried out on pure Si surfaces under low-pressure conditions. It is well-known, however, that Si can also easily be oxidized in air, even at room temperature, covering the surface by an ultrathin oxide layer (the so-called "native" oxide) with a thickness of up to 1 nm.[5] However, this native oxide layer is a poor dielectric. Therefore, such oxide layers usually need to be removed prior to oxidation for their use in the microelectronics technology.[6] Hyperthermal oxidation of a Si surface covered with its native oxide may provide an alternative to this process as well as control of ultrathin thickness of such oxide even at low temperature.

Moreover, knowledge of the interaction of hyperthermal oxygen with a native silicon oxide layer is also of particular importance for space travel.[7] Si is one of the most widely used materials for space crafts, and therefore, a native oxide layer can also be found on spacecraft material. When the spacecraft travels in the ionosphere, which consists of many hyperthermal species (∼5 eV) including oxygen atoms and molecules, these hyperthermal particles can seriously damage its surface. Due to this hyperthermal bombardment, the material properties can be altered.[8] An atomic-scale understanding of the corresponding oxidation processes and mechanisms, as well as an analysis of the obtained ultrathin structures, is therefore very useful.

The already existing models describing thermal oxidation mechanisms, including Deal−Grove and its extensions,[9,10] "reactive layer",[11] and Cabrera−Mott mechanisms[12] are inappropriate to properly describe the initial stage of hyperthermal Si oxidation.[8,13,14] Therefore, several alternative mechanisms have been presented describing the onset of hyperthermal oxidation of Si surfaces.[4,8,14,15] However, there are still many unresolved questions, and detailed knowledge of the mechanisms is still lacking.[13] For instance, the oxidation process by which the native oxide is further oxidized is still unclear. In order to unravel the oxidation mechanisms as well as to gain a more fundamental understanding of the onset of hyperthermal oxidation of a native oxide film, this work continues on our previous studies and focuses on the atomic-scale dynamics underpinning the oxidation process.

■ COMPUTATIONAL DETAILS

The hyperthermal oxidation process is investigated at the atomic scale by reactive molecular dynamics (MD) simulations,

Received: January 14, 2013
Revised: April 22, 2013
Published: April 23, 2013

 © 2013 American Chemical Society dx.doi.org/10.1021/jp400433u | J. Phys. Chem. C 2013, 117, 9819−9825

employing the reactive force field (ReaxFF).[16] The ReaxFF potential uses the concept of partial bond orders to accurately model bond breaking and bond formation and is based on the bond length−bond order/bond order−bond energy relationship introduced by Abell.[17] Our previous studies[14,18−20] indicated that ReaxFF accurately describes bond breaking and formation as well as the expansion of the Si crystal during the oxide formation process. As a result, the direct oxidation behavior and *a*-SiO_2 formation as well as control of the oxide thickness in hyperthermal Si oxidation were successfully explained. The obtained results were in good agreement with both experimental and density functional theory (DFT) results in similar cases. A detailed description of the force field as developed for the Si|SiO_2 system can be found elsewhere.[16,21,22] In this work, we use the force field parameters developed by Buehler et al.[22]

As our goal is to fundamentally understand the hyperthermal oxidation of a native oxide film, we first simulate the formation of such a thin oxide layer as follows. A Si(100){2 × 1} reconstructed surface (*c*-Si, shown in Figure 1) is chosen as the initial structure, with dimensions 21.7 Å × 21.7 Å × 27.1 Å. This structure is oxidized by 1 eV oxygen molecules at room temperature. More details on this oxidation process can be found elsewhere.[19] The resulting structure is subsequently equilibrated at 300, 700, and 900 K using the Berendsen heat bath (NVT dynamics)[23] for 20 ps with a damping constant of 0.1 ps. Next, the three obtained structures are relaxed in the microcanonical ensemble (NVE dynamics) for 10 ps. Note that, although the Berendsen heat bath does not generate a canonical ensemble, we found no significant differences in results as obtained using the Berendsen and the canonical Bussi thermostat.[24]

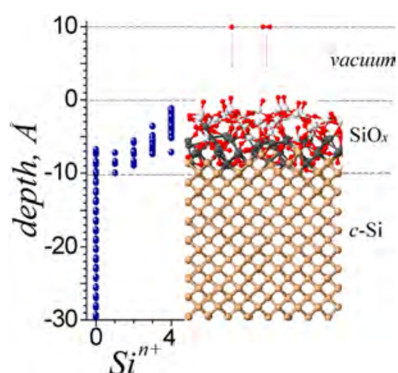

Figure 1. SiO_x|*c*-Si structure prior to oxidation. The projectile (O or O_2—red atoms) is initially positioned 10 Å above the surface. The morphology of the structure is analyzed by silicon (sub)oxide components. Dark gray atoms indicate silicon suboxide species.

In Figure 1, the resulting SiO_x structure, covering the Si crystal, is depicted. We analyzed this structure by means of the silicon (sub)oxide components.[19] Here, the Si^{1+}, Si^{2+}, Si^{3+}, and Si^{4+} components arise from interfacial silicon atoms, which bind to one, two, three, and four nearest-neighbor oxygen atoms, respectively, and thus correspond to Si_2O, SiO, Si_2O_3, and SiO_2, respectively.[25] Note that the notation used corresponds to formal charge states and not to the actual atomic charges. The figure shows that the silicon (sub)oxide components are consecutively distributed in the SiO_x ($x < 2$) nonstoichiometric (gray atoms or Si^{1+}, Si^{2+}, and Si^{3+}) and SiO_2 stoichiometric (white atoms or Si^{4+}) oxide regions. Our previous studies showed that the stoichiometric silica structure is amorphous (*a*-SiO_2).[14,19] As some high-order silicon suboxide components, e.g., Si^{3+}, can also be found in the *a*-SiO_2 region, we simply designate both oxide regions as SiO_x ($x \leq 2$).

Also, our previous study showed that the average partial charges are about +1.2 and −0.6 in SiO_2 for Si and O atoms, while they range from 0.0 to +1.2 and from −0.9 to −0.6, respectively, in the Si|SiO_2 interface.[19] Note that the calculated charges are determined from the electronegativity equalization method (EEM) method, fitted to Mulliken charges.[16] As Mulliken charges are heavily dependent on the basis set used, the exact values should not be taken too literally. Nevertheless, the obtained values are in reasonably good agreement with experimental values for SiO_2 quartz and coesite.[26]

Hyperthermal oxygen impacts are subsequently performed as follows. The incident particle (oxygen atom or oxygen molecule) is positioned at a *z*-position of 10 Å above the SiO_x surface. The vacuum above the surface are chosen big enough (∼50 Å in the *z*-direction) to ensure that the top of the surface does not interact with the bottom of the structure through the *z*-periodic boundary. The {*x*, *y*} coordinates of the incident particle are chosen randomly. In the case of molecular oxygen, the O_2 molecule is rotated randomly prior to impact. The impinging particle is directed normal to the surface, corresponding to laser detonation experiments.[4,27] All impacts are nonconsecutive, i.e., each impact occurs on the original native silicon oxide surface, and they are monitored in the range of 3−25 ps depending on the observed processes. The initial kinetic energies of the oxygen species (O, O_2) are set to 1 and 5 eV. Each case is repeated 1000 times to gather statistically valid results.

■ RESULTS AND DISCUSSION

1. Initial Reactions. The probabilities of oxygen atoms or molecules to be found in three different regions, after impact on the *a*-SiO_2 surface, are presented in Table 1, for both atomic and molecular impacts at two different energies and three different substrate temperatures, as based on 1000 nonconsecutive impacts as mentioned above.

Table 1. Probabilities of the Final Positions of the Projectiles (O or O_2) in Three Different Regions after Impact on the *a*-SiO_2 Surface

	atomic						molecular					
	1 eV			5 eV			1 eV			5 eV		
	300 K	700 K	900 K	300 K	700 K	900 K	300 K	700 K	900 K	300 K	700 K	900 K
vacuum	0.155	0.074	0.060	0.070	0.060	0.015	0.970	0.950	0.930	0.780	0.760	0.742
SiO_x	0.845	0.926	0.940	0.930	0.935	0.975	0.030	0.050	0.070	0.220	0.240	0.258
c-Si	0	0	0	0	0.005	0.010	0	0	0	0	0	0.001

1.1. Scattering Probabilities. The designation "vacuum" means that the oxygen particle was reflected from the surface. The results in Table 1 clearly show that impacting O_2 molecules mostly scatter from the SiO_2 surface. The scattering rate decreases somewhat with increasing impact energy and substrate temperature. This rate decreases very slowly at about 1% per 100 K or 5% per 1 eV. In most cases (~94%), molecules scatter without breaking up. Interestingly, this percentage is almost constant for all temperatures and energies. Such behavior is well-known for O_2 interacting with Si surfaces during thermal as well as hyperthermal oxidation[13] and has been shown to be dependent on the molecular orientation, i.e., O_2 molecules parallel to the surface are more reactive than molecules oriented perpendicular to the surface.[28] For atomic impacts, however, the scattering probability is significantly lower than in the molecular case. The percentage of reflected atoms due to atomic impacts never exceeds 15%.

1.2. Sticking Probabilities. In contrast to the molecular impacts, it is clear from Table 1 that the oxygen sticking probabilities during atomic impacts are in general very high and gradually increase with increasing incident energy and surface temperature. Vice versa, the molecular sticking probability is very low, as analyzed above. Most of the sticking O_2 molecules adsorb dissociatively at higher temperatures (700 and 900 K). At least 75% of the sticking molecules break up and penetrate the structure as separate atoms after impact on the *a*-SiO_2 surface. On the other hand, at room temperature, this percentage significantly drops from 50% to only 3% with impact energy decreasing from 5 to 1 eV. In contrast, our previous investigations showed that the oxygen sticking probability on *c*-Si is very high, both for atomic as well as molecular oxygen.[18]

Furthermore, the probabilities to find O in the *c*-Si region are not zero for 5 eV impacts at high temperature, both for atomic (up to 1%) as well as molecular impacts (only one case). Indeed, the adsorbing particles can react with the crystal surface after diffusing through the SiO_x layer. This oxidation behavior is very similar to thermal oxidation, as discussed in the next sections.

These results show that scattering and sticking rates of the incident species depend on the type of the incident oxygen species, their incident energy, and on the bulk temperature. These parameters can therefore control the onset of the oxidation process of the native oxide layer.

2. Penetration Depth. In Figure 2, the calculated normalized penetration probability distributions are plotted for atomic and molecular oxygen at different impact energies and oxidation temperatures. In the figure, the positions at 0 Å and about −10 Å correspond to the average *z*-coordinate of the atoms at the SiO_x ($x \leq 2$) surface and at the SiO_x|*c*-Si interface, respectively (see also Figure 1).

As presented in the previous section, the total fraction of the penetrated atoms in the SiO_x region in the case of molecular impacts is in the range of 3−26%, which is significantly less than in the case of atomic impacts (~85−98%; see Table 1). Therefore, for the sake of clarity, the penetration probabilities are normalized for both impact cases.

The figure illustrates that the penetration depth increases with increasing impact energy and increasing substrate temperature. The analysis of the penetration probability distribution reveals that implanted oxygen atoms or molecules preferentially reside close to the surface in the case of molecular 1 eV impacts at 300 K. Also, for both atomic and molecular

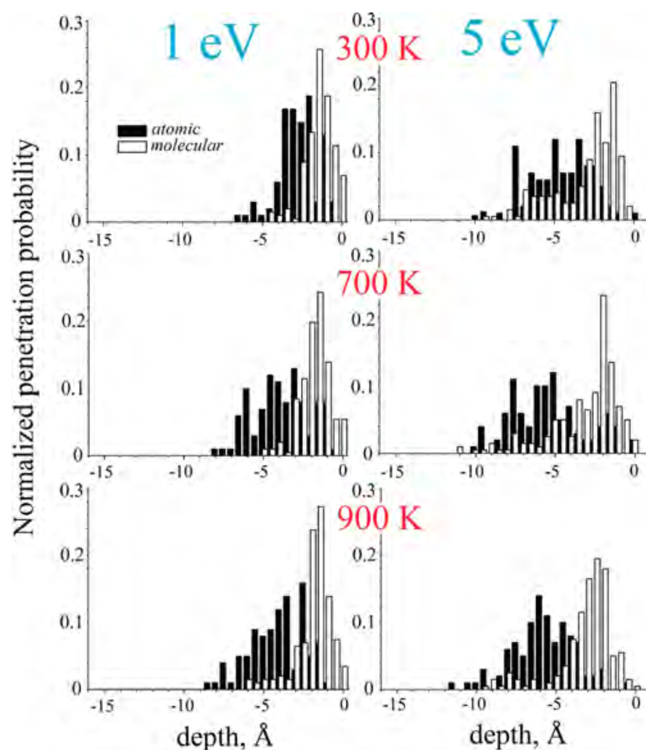

Figure 2. Calculated normalized penetration depth distributions for atomic (black bars) and molecular (white bars) impacts with 1 and 5 eV at three different surface temperatures. On the *x*-axis, $z = 0$ Å and $z = -10$ Å correspond to the average *z*-coordinate of the atoms at the *a*-SiO_2 surface and the SiO_x|*c*-Si interface.

impacts with an impact energy of 1 eV, all penetrated oxygen species are found only in the SiO_x ($x \leq 2$) oxide region, close to the *a*-SiO_2|SiO_x interface. Comparing the atomic impacts with the molecular impacts, we find that the implanted atoms penetrate somewhat deeper at both 1 and 5 eV in the case of atomic impacts, as shown in the figure. Indeed, the molecules are given the same initial kinetic energy as the atoms, such that the individual atoms obtained after dissociation have less momentum and hence a lower velocity than the atoms in the atomic impacts. Therefore, they do not penetrate as deep in the oxide as the oxygen atoms originating from atomic impacts. This oxidation behavior was also found in our previous work on hyperthermal oxygen interacting with *c*-Si (100) surfaces.[18] In that case, however, they easily penetrate into the first subsurface layer of the Si bulk in absence of a surface energy barrier.[18] Therefore, the penetration depth strongly depends on the first and second subsurface energy barriers, estimated to be 1.0 and 2.4 eV, respectively.[8,18,29] In the present case, on the other hand, oxygen should first penetrate and overcome the oxide barrier before it can react with the Si crystal. Therefore, in most cases, the penetrated oxygen atoms reside in the oxide region.

Also, Figure 2 indicates that oxygen atoms with an impact energy of 5 eV can also be found deeper in the SiO_x region, as well as in the SiO_x|*c*-Si interface region, at higher temperatures starting from 700 K. Furthermore, the results show that the penetration depth is controlled by the impact energy of the impinging species, rather than by the oxidation temperature in the initial stage. After this initial stage (which lasts for about 0.5 ps), however, the temperature plays an important role in allowing the oxygen atoms to overcome the SiO_x|*c*-Si interface "barrier" and react with the Si crystal. At low temperature, on

the other hand, an increase in the interfacial stress is found to lead to a decrease in the oxidation rate.[20]

3. Oxidation Mechanisms. *3.1. "Common Oxidation" (CO) Mechanism.* As discussed in the previous section, the penetrating oxygen atoms mostly end up in the non-stoichiometric part of the SiO_x region, after crossing the ultrathin a-SiO_2 layer, at both impact energies and for all temperatures investigated. Analysis of this penetration behavior may provide useful information for understanding the onset of the hyperthermal oxidation of the oxygenated Si surface.

The oxygen penetration is schematically presented in Figure 3 for an atomic impact with an impact energy of 5 eV at a substrate temperature of 300 K. This process is observed for both atomic and molecular impacts with energies of 1 and 5 eV at all three oxidation temperatures. In the figure, the mechanism is represented as a time evolution of the kinetic energy (E_{kin}), bond order (BO), and penetration depth (z) of the projectile. We distinguish four stages in the mechanism, i.e., the oxidant behavior before the impact (I), interaction with the a-SiO_2 surface and penetration in the a-SiO_2 region (II), penetration and reaction with the SiO_x ($x < 2$) region (III), and the final stage where the impinging particle is thermalized (IV).

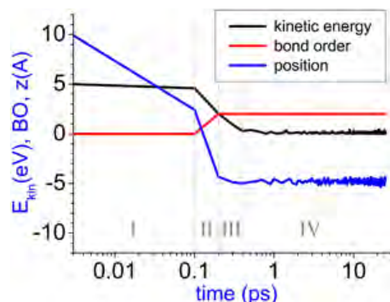

Figure 3. Time evolution of the oxygen kinetic energy E_{kin}, bond order BO, and penetration depth z, as an illustration for the "common oxidation" (CO) mechanism. The averaged z-coordinates of the atoms on the a-SiO_2 surface and on the a-$SiO_2|SiO_x$ ($x < 2$) interface correspond to 0 and about −5 Å, respectively. Note that some Si^{i+} ($i < 4$) atoms are also found in the a-SiO_2 region (see also Figure 1). See text for a discussion of stages I−IV.

The projectile is initially positioned at 10 Å above the surface. In stage I, the projectile motion is uniform, i.e., it moves along a straight line (normal to the surface) with a constant velocity equal to about 78 Å/ps (7.8 km/s). Of course, the initial energy (E_{kin} = 5 eV) and bond order (BO = 0) remain constant as well in this period. When the impinging particle interacts with the surface atoms, its kinetic energy drops to about 2 eV in stage II. At the end of this stage, the bond order of the particle reaches its final average value of 2 (i.e., the O atom is bonded with two Si atoms). In the third stage, the penetrating projectile crosses the a-$SiO_2|SiO_x$ interface, reacts with Si^{i+} ($i < 4$) atoms, and reaches its maximum depth in the nonstoichiometric SiO_x region. Here, the implanting atom uses its residual energy to diffuse in the a-SiO_2 region before binding to a suboxide Si atom. Also, depending on the residual energy, the oxidant penetrates deeper in the nonstoichiometric SiO_x region, even up to the $SiO_x|c$-Si interface. However, a reaction with c-Si does not occur in this oxidation mechanism. Furthermore, in some 1 eV impact cases at room temperature, the oxygen atoms do not penetrate further and thus react in the a-SiO_2 region, leading to defect creation in this region (e.g., peroxyl oxygen bonds, oxygen-deficient Si centers etc., as explained in section 4 below).[30] Indeed, defect creation is most prominent at low temperature. Finally, in the fourth stage, the kinetic energy as well as the position and bond order of the particle remain constant. In this stage, the impinging particle is fully thermalized.

3.2. Thermal-Like Oxidation (TLO) Mechanism. At higher temperatures, especially starting from about 700 K (see Table 1, c-Si), some oxygen atoms or molecules penetrate down to the $SiO_x|c$-Si interface and react with the Si crystal. As mentioned in section 1, the probability for an oxygen atom to reach this interface is only in the 1% range. Interestingly, the oxidation mechanism of such oxygen species resembles thermal oxidation, which is described by the Deal−Grove model: oxygen reacts with the Si crystal after diffusing through the oxide layers.[9] The TLO mechanism is schematically represented in Figure 4a.

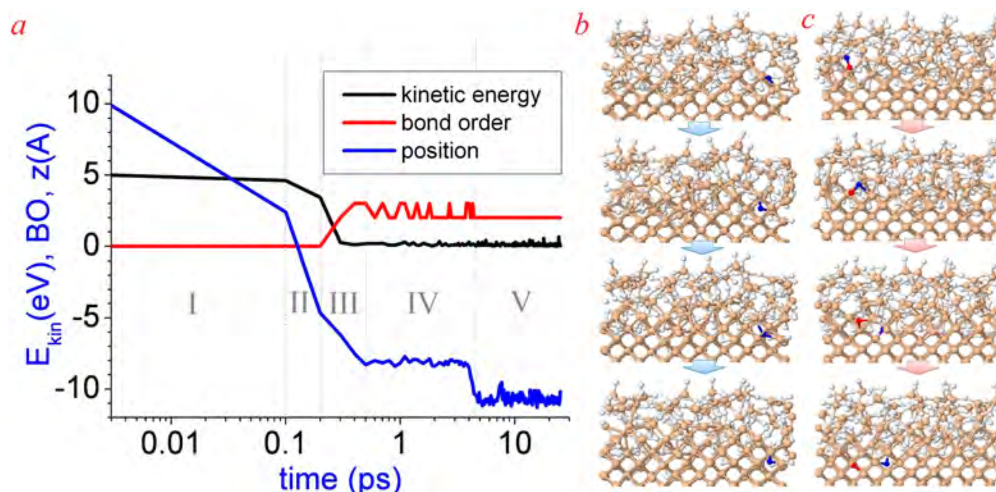

Figure 4. Thermal-like oxidation (TLO) mechanism: (a) time evolution of penetration depth z, kinetic energy E_{kin}, and bond order BO. In this mechanism, atomic (b) or molecular (c) oxygen can react with the c-Si surface by penetrating through the nonstoichiometric SiO_x oxide region at temperatures of 700 K and above. See text for a discussion of stages I−V.

dx.doi.org/10.1021/jp400433u | J. Phys. Chem. C 2013, 117, 9819−9825

This mechanism can be explained by division of the time evolution into five stages. The first two stages are very similar to the corresponding stages in the CO mechanism discussed above. However, in stage III, the penetrating oxidant particles continue traveling in the direction along the *z*-axis in the SiO_x region and interact with Si^{i+} ($i < 4$) atoms near the SiO_x|*c*-Si interface.

Note that, in both mechanisms, the projectile (O or O_2) loses a significant fraction of its initial kinetic energy in the second and third stages. The corresponding stopping powers (or energy loss per depth) are about 0.27 eV/Å (20 eV/ps) and 0.83 eV/Å (30 eV/ps) during stages II and III of the thermal-like mechanism, whereas they are about 0.43 eV/Å (30 eV/ps) and 4 eV/Å (20 eV/ps) in the CO mechanism in the same stages. Thus, the oxygen in stage III can penetrate deeper into the structure, up to the SiO_x|*c*-Si interface in the TLO mechanism, as mentioned above, while it can only reach the *a*-SiO_2|SiO_x interface in the CO mechanism due to the higher stopping power. Indeed, in stages II and III of both oxidation mechanisms, oxygen species can directly oxidize subsurface layers of the SiO_x oxide. These two initial stages therefore correspond to the direct oxidation period[14,18] and take about 0.5 ps, as shown in Figures 3 and 4. During this short period, physisorption (mostly in stage II) and chemisorption processes (mostly in stage III) can "directly seed" the oxygen species in the oxygenated Si. Thus, the initial stage of the hyperthermal oxidation of a native silicon oxide film is significantly different from the onset of thermal oxidation, which only commences after an "incubation period".[31]

Furthermore, while the energy and position of the implanting oxygen species along the *z*-axis remain constant in stage IV of the TLO mechanism, like in the CO mechanism, this stage is still not similar to the corresponding stage in the CO mechanism. Indeed, in this stage, the bond order of the oxidant fluctuates in the TLO mechanism, indicating that the resulting configuration is unstable, in contrast to the CO mechanism. Thus, this depth is not necessarily the final depth of the particle. The oxidant can diffuse on a short time scale until the bond order stabilizes. As mentioned in the CO mechanism, the diffusion rate for the oxidant is very low at low temperatures. Finally, in stage V, the oxidant reacts with the *c*-Si, after which the energy, position, and bond order remain constant with negligible fluctuations. This stage is similar to stage IV of the CO mechanism.

A schematic picture of the TLO mechanism is shown in Figure 4b as well as Figure 4c: the oxygen atom or molecule penetrates through the oxide region and eventually reacts with the Si crystal. The frames shown describe the position of the oxygen particle in the various stages, i.e., stages II−V.

Thus, in the TLO mechanism, five stages can be discerned, i.e., motion prior to impact (I), interaction with the *a*-SiO_2 surface and penetration into this region (II), penetration and weak interactions with Si atoms in the SiO_x ($x < 2$) region near the SiO_x|*c*-Si interface (III), diffusion toward the SiO_x|*c*-Si interface (IV), and finally reaction with *c*-Si (V).

Previously, we also presented temperature-dependent mechanisms for oxidation of pure (i.e., nonoxidized) Si(100) surfaces using hyperthermal oxygen atoms and molecules.[14,19] We found that the hyperthermal oxidation mechanism is significantly different from other thermal oxidation mechanisms including the Deal−Grove model (i.e., downward oxygen diffusion)[9] and the "reactive layer" model (i.e., upward Si diffusion).[11] Indeed, in the hyperthermal oxidation mechanism of pure Si surfaces, the projectile cannot diffuse through the nonstoichiometric SiO_x region, which has a thickness above 1 nm, and thus cannot react with the crystalline Si surface, even at high temperature (e.g., 1300 K).[14] Note, however, that this oxidation behavior is very similar to the CO mechanism for native oxide surfaces (see Figure 3 above). In contrast, in the TLO mechanism, the high impact energy and higher bulk temperature help the impinging O species to cross the somewhat thinner SiO_x region and react with the crystal. This result is in close agreement with experimental evidence for thermal oxidation, demonstrating that the interstitial neutral oxygen atoms and molecules become mobile above 200 °C (∼500 K) and 400 °C (∼700 K), respectively.[30]

4. Defect Formation Processes. During oxidation, the impinging oxygen species can create defects in the oxide region. Two main defect formation processes are observed. The first mechanism described below corresponds to molecular impacts and the second mechanism to atomic impacts. In the first process, the incident molecule reacts with a silicon epoxide structure (i.e., "green Si"−O−"gray Si" triangular configuration, denoted by SiØSi)[32] near the *a*-SiO_2|SiO_x interface as shown in Figure 5a. Note that the SiØSi structures are mostly found in the nonstoichiometric oxide region. The creation of such intrinsic defects can be explained by a physical stress-enhanced bond breaking mechanism: the number of Si−Si bonds increases in the SiO_x oxide when the stress increases.[20,33] The penetrating atom or molecule does not react with the crystal at low temperature, because of compressive interfacial stresses.[20] When an oxygen molecule interacts with one of the Si atoms of such a silicon epoxide structure, the Si−Si bond in this structure is broken. The O_2 molecule subsequently binds weakly (physisorption) with the suboxide Si component (Si^{3+}) creating an oxygen defect. As a result, the O−O distance in the molecule becomes somewhat longer and the molecule converts to a peroxide. The partial radial distribution function (RDF), as presented in Figure 5c, shows that the maximum of the O−O distance (first peak) in the oxygen peroxides is about 1.25 Å, which is slightly longer that the interatomic distance in the O_2 molecule (1.21 Å).

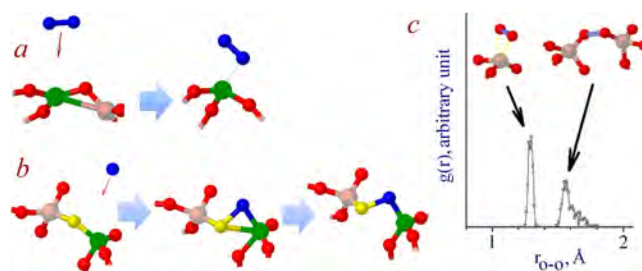

Figure 5. Two types of defect creation mechanisms in molecular (a) and atomic (b) impacts. Reacting Si and O atoms in the initial structures are colored in green and yellow, respectively, while the incident particles are colored blue. (c) Partial radial distribution function (RDF) of the O−O distance, showing these defects (i.e., oxygen peroxyl bonds) in the SiO_x ($x \leq 2$) oxide region, i.e., the first peak in the RDF corresponds to the defect of panel a, and the second to the defect of panel b.

The calculation shows that the formation energy of the defect is −1.093 eV/atom. This defect is thus found to be stable. Also, the energy barriers for the defect formation were calculated with ReaxFF using the nudged-elastic-band (NEB) method.[34] The barrier (activation) energies for forward and

backward reactions are calculated as 1.43 and 1.99 eV/atom, respectively. At high temperature (∼700 K), however, this type of defect (i.e., oxygen deficiency) becomes unstable, and such peroxyl bonds in the defect structure can easily diffuse in the nonstoichiometric SiO_x oxide.

Furthermore, the RDF also indicates that somewhat different oxygen peroxyl bridges can be found in the stoichiometric oxide region as well. In Figure 5c, it can be seen that the maximum of the O−O distance (second peak) in oxygen peroxyl bonds for the second defect structures is about 1.56 Å, which is somewhat longer than the O−O distance in peroxyl bonds in the first defect structure. In the second defect formation process (Figure 5b), which is observed only during atomic impacts, the incident atom reacts with Si^{4+} atoms and creates oxygen peroxyl bonds in the *a*-SiO_2 region. In this process, the Si^{4+} atom becomes an overcoordinated Si^{5+} atom when connecting with the incoming oxygen (see Figure 5b, "green Si" in the middle structure). In this triangular Si−O−O structure, the old Si−O bond breaks up when the new Si−O bond forms. The old Si−O bond thus becomes somewhat weaker when the O reacts with a "guest" oxygen. As a result, two SiO_2 molecules in the stoichiometric oxide region connect to each other through a O−O bond, creating a Si deficiency in this region. These defects can therefore decrease the oxide (or silica) mass density.[35] These defects are, however, unstable. We calculated the defect formation energy to be 1.017 eV/atom and the forward and backward reaction activation (barrier) energies as 1.02 eV/atom and 2.25 eV/atom, respectively.

Note that both defect formation processes mostly occur at low temperatures. This can be explained by the high compressive stresses in the oxide (although tensile stresses dominate on the surface).[36,37] When the oxidation temperature increases, the number of the oxygen peroxyl bridges decreases significantly.[14]

CONCLUSIONS

The structure of ultrathin silicon oxide films, which is critical for, e.g., the MOSFET gate oxide, is strongly dependent on the oxidation mechanism. Here, we studied the oxidation of a *a*-SiO_2|SiO_x|*c*-Si structure, with a 1 nm native oxide (*a*-SiO_2|SiO_x) surface layer, by hyperthermal oxygen atoms and molecules using reactive molecular dynamics simulations.

The results showed that the onsets of hyperthermal and thermal oxidation are significantly different, due to the direct oxidation behavior of the hyperthermal oxygen species. In the initial "direct oxidation" period (∼0.5 ps), the reacting oxygen atom (or molecule) can immediately reach its final depth in the nonstoichiometric SiO_x oxide region. Because of their high sticking rate, hyperthermal oxygen atoms oxidize the SiO_x region very effectively. In contrast, the molecular sticking rate is very low, and in most cases the impinging molecules break up.

Two different oxidation mechanisms were observed: the CO mechanism and a TLO mechanism. In the CO mechanism, the oxidation process proceeds by oxidation of the SiO_x region, whereas the TLO mechanism proceeds by oxidation of the crystalline Si (*c*-Si) region. The TLO mechanism was observed to occur at higher temperature starting at about 700 K. This model is thus similar to the traditional thermal Si oxidation as described by the Deal−Grove model, at least when neglecting the direct oxidation stage.

Finally, some defect formation processes, which are responsible for local Si and O deficiencies in the oxide, are also discussed. Defects are mainly created in the SiO_x region, and mostly at low temperature, due to the compressive stresses in the oxide region.

These results are of importance for the fabrication of silica-based devices in the micro- and nanoelectronics industry as well as for spacecraft investigations.

AUTHOR INFORMATION

Corresponding Author

*Phone: +32-3-265-23-82. Fax: +32-3-265-23-43. E-mail: umedjon.khalilov@ua.ac.be.

Notes

The authors declare no competing financial interest.

ACKNOWLEDGMENTS

U.K. acknowledges IMEC for financial support. A.C.T.v.D. acknowledges funding from the Air Force Office of Scientific Research (AFOSR) under Grant No. FA9550-10-1-0563. G.P. acknowledges funding from the European Project 2D-NANO-LATTICES under the FET Grant No. 270749. The authors also gratefully acknowledge financial support from the Fund for Scientific Research (FWO-Vlaanderen). This work was carried out in part using the Turing HPC infrastructure at the CalcUA core facility of the Universiteit Antwerpen (UA), a division of the Flemish Supercomputer Center VSC, funded by the Hercules Foundation, the Flemish Government (department EWI), and the UA.

REFERENCES

(1) Schulz, M. The End of the Road for Silicon? *Nature* **1999**, *399*, 729−730.

(2) Gibson, J. M.; Lanzerotti, M. Y. Observation of Interfacial Atomic Steps during Silicon Oxidation. *Nature* **1989**, *340*, 128−131.

(3) Green, M. L.; Gusev, E. P.; Degraeve, R.; Garfunkel, E. L. Ultrathin (<4 nm) SiO_2 and Si−O−N Gate Dielectric Layers for Silicon Microelectronics: Understanding the Processing, Structure, and Physical and Electrical Limits (Review). *J. Appl. Phys.* **2001**, *90*, 2057.

(4) Tagawa, M.; Ema, T.; Kinoshita, H.; Ohmae, N.; Umeno, M.; Minton, T. K. Formation of Thin Oxide Films on Room-Temperature Silicon (100) by Exposure to a Neutral Beam of Hyperthermal Atomic and Molecular Oxygen. *Jpn. J. Appl. Phys.* **1998**, *37*, L1455−L1457.

(5) Morita, M.; Ohmi, T.; Hasegawa, E.; Kawakami, M.; Ohwada, M. Growth of Native Oxide on a Silicon Surface. *J. Appl. Phys.* **1990**, *68*, 1272.

(6) Chin, A.; Chen, W. J.; Chang, T.; Kao, R. H.; Lin, B. C.; Tsai, C.; Huang, J. C.-M. Thin Oxides with in Situ Native Oxide Removal [n-MOSFETs]. *IEEE Electron Device Lett.* **1997**, *18*, 417−419.

(7) Murad, E. Spacecraft Interaction with Atmospheric Species in Low Earth Orbit. *J. Spacecr. Rockets* **1996**, *33*, 131−136.

(8) Kisa, M.; Minton, T. K.; Yang, J. C. Structural Comparisons of SiO_x and Si/SiO_x Formed by the Exposure of Silicon (100) to Molecular Oxygen and to Hyperthermal Atomic Oxygen. *J. Appl. Phys.* **2005**, *97*, 023520.

(9) Deal, B. E.; Grove, A. S. General Relationship for the Thermal Oxidation of Silicon. *J. Appl. Phys.* **1965**, *36*, 3770−3778.

(10) Massoud, H. Z.; Plummer, J. D.; Irene, E. A. Thermal Oxidation of Silicon in Dry Oxygen: Growth-Rate Enhancement in the Thin Regime. II. Physical Mechanisms. *J. Electrochem. Soc.* **1985**, *132*, 2693.

(11) Mott, N. F.; Rigo, S.; Rochet, F.; Stoneham, A. M. Oxidation of Silicon. *Philos. Mag.* **1989**, *60*, 189−212.

(12) Cabrera, N.; Mott, N. F. Theory of the Oxidation of Metals. *Rep. Prog. Phys.* **1949**, *12*, 148.

(13) Okada, M. Surface Chemical Reactions Induced by Well-Controlled Molecular Beams: Translational Energy and Molecular Orientation Control (Topical Review). *J. Phys.: Condens. Matter* **2010**, *22*, 263003.

(14) Khalilov, U.; Pourtois, G.; van Duin, A. C. T.; Neyts, E. C. Hyperthermal Oxidation of Si(100)2 × 1 Surfaces: Effect of Growth Temperature. *J. Phys. Chem. C* **2012**, *116*, 8649−8656.
(15) Yoshigoe, A.; Teraoka, Y. Time Resolved Photoemission Spectroscopy on Si(001)-2 × 1 Surface during Oxidation Controlled by Translational Kinetic Energy of O_2 at Room Temperature. *Surf. Sci.* **2003**, *532−535*, 690−697.
(16) van Duin, A. C. T.; Strachan, A.; Stewman, S.; Zhang, Q.; Xu, X.; Goddard, W. A., III. $ReaxFF_{SiO}$ Reactive Force Field for Silicon and Silicon Oxide Systems. *J. Phys. Chem. A* **2003**, *107*, 3803−3811.
(17) Abell, G. C. Empirical Chemical Pseudopotential Theory of Molecular and Metallic Bonding. *Phys. Rev. B* **1985**, *31*, 6184−6196.
(18) Neyts, E. C.; Khalilov, U.; Pourtois, G.; van Duin, A. C. T. Hyperthermal Oxygen Interacting with Silicon Surfaces: Adsorption, Implantation, and Damage Creation. *J. Phys. Chem. C* **2011**, *115*, 4818−4823.
(19) Khalilov, U.; Neyts, E. C.; Pourtois, G.; van Duin, A. C. T. Can We Control the Thickness of Ultrathin Silica Layers by Hyperthermal Silicon Oxidation at Room Temperature? *J. Phys. Chem. C* **2011**, *115*, 24839−24848.
(20) Khalilov, U.; Pourtois, G.; van Duin, A. C. T.; Neyts, E. C. On the *c*-Si|*a*-SiO_2 Interface in Hyperthermal Si Oxidation at Room Temperature. *J. Phys. Chem. C* **2012**, *116*, 21856−21863.
(21) Fogarty, J. C.; Aktulga, H. M.; Grama, A. Y.; van Duin, A. C. T.; Pandit, S. A Reactive Molecular Dynamics Simulation of the Silica−Water Interface. *J. Chem. Phys.* **2010**, *132*, 174704.
(22) Buehler, M. J.; van Duin, A. C. T.; Goddard, W. A., III. Multi-Paradigm Modeling of Dynamical Crack Propagation in Silicon Using the ReaxFF Reactive Force Field. *Phys. Rev. Lett.* **2006**, *96*, 95505.
(23) Berendsen, H. J. C.; Postma, J. P. M.; van Gunsteren, W. F.; Di Nola, A.; Haak, J. R. Molecular Dynamics with Coupling to an External Bath. *J. Chem. Phys.* **1984**, *81*, 3684−3690.
(24) Bussi, G.; Donadio, D.; Parrinello, M. Canonical Sampling through Velocity Rescaling. *J. Chem. Phys.* **2007**, *126*, 014101.
(25) Oh, J. H.; Nakamura, K.; Ono, K.; Oshima, M.; Hirashita, N.; Niwa, M.; Toriumi, A.; Kakizaki, A. Initial Oxidation Features of Si(100) Studied by Si2p Core-Level Photoemission Spectroscopy. *J. Electron Spectrosc. Relat. Phenom.* **2001**, *114−116*, 395−399.
(26) Newton, M. D.; Gibbs, G. V. Ab Initio Calculated Geometries and Charge Distributions for H_4SiO_4 and $H_6Si_2O_7$ Compared with Experimental Values for Silicates and Siloxanes. *Phys. Chem. Miner.* **1980**, *6*, 221−246.
(27) Caledonia, G. E.; Krech, R. H.; Green, B. D. A High Flux Source of Energetic Oxygen Atoms for Material Degradation Studies. *AIAA J.* **1987**, *25*, 59.
(28) Kurahashi, M.; Yamauchi, Y. Huge Steric Effects in Surface Oxidation of Si(100). *Phys. Rev. B* **2012**, *85*, 161302.
(29) Kato, K.; Uda, T.; Terakura, K. Backbond Oxidation of the Si(001) Surface: Narrow Channel of Barrierless Oxidation. *Phys. Rev. Lett.* **1998**, *80*, 2000.
(30) Kajihara, K.; Miura, T.; Kamioka, H.; Aiba, A.; Uramoto, M.; Morimoto, Y.; Hirano, M.; Skuja, L.; Hosono, H. Diffusion and Reactions of Interstitial Oxygen Species in Amorphous SiO_2: A Review. *J. Non-Cryst. Solids* **2008**, *354*, 224−232.
(31) Massoud, H. Z. Thermal Oxidation of Silicon in the Ultrathin Regime. *Solid-State Electron.* **1997**, *41*, 929−934.
(32) Stefanov, B. B.; Gurevich, A. B.; Weldon, M. K.; Raghavachari, K.; Chabal, Y. J. Silicon Epoxide: Unexpected Intermediate during Silicon Oxide Formation. *Phys. Rev. Lett.* **1998**, *81*, 3908−3911.
(33) Yang, T.-C.; Saraswat, K. C. Effect of Physical Stress on the Degradation of Thin SiO_2 Films under Electrical Stress. *IEEE Trans. Electron Devices* **2000**, *47*, 746−755.
(34) Henkelman, G.; Uberuage, B. P.; Jonsson, H. A Climbing Image Nudged Elastic Band Method for Finding Saddle Points and Minimum Energy Paths. *J. Chem. Phys.* **2000**, *113*, 9901−9904.
(35) Ng, K.-O.; Vanderbilt, D. Structure and Oxidation Kinetics of the Si(100)−SiO_2 Interface. *Phys. Rev. B* **1999**, *59*, 10132−10137.
(36) Donnadieu, P.; Blanquet, E.; Jakse, N.; Mur, P. Detection of Subnanometric Layer at the Si/SiO_2 Interface and Related Strain Measurements. *Appl. Phys. Lett.* **2004**, *85*, 5574−5576.
(37) Kao, D.-B.; McVittie, J. P.; Nix, W. D.; Saraswat, K. C. Two-Dimensional Thermal Oxidation of Silicon—II. Modeling Stress Effects in Wet Oxides. *IEEE Trans. Electron Devices* **1988**, *35*, 25−37.